Electronic Supplementary Material (ESI) for Journal of Materials Chemistry A.
This journal is © The Royal Society of Chemistry 2022

Supporting Information

In-situ thermal exclusion induced Sb and Sb-doped SnO_2 nanoheterostructuring and its improvements in cycling stabilities and rate capacities for Na^+ storage

Liping Guo,[a] Zhong-Jie Jiang,[*,a] Yongjie Wang,[b] Zhongqing Jiang[c]

[a] *Guangzhou Key Laboratory for Surface Chemistry of Energy Materials, Guangdong Engineering and Technology Research Center for Surface Chemistry of Energy Materials, College of Environment and Energy, South China University of Technology, Guangzhou 510006, P. R. China. E-mail: eszjiang@scut.edu.cn and zhongjiejiang1978@hotmail.com*

[b] *School of Science, Harbin Institute of Technology, Shenzhen 518055, P. R. China.*

[c] *Key Laboratory of Optical Field Manipulation of Zhejiang Province, Department of Physics, Zhejiang Sci-Tech University, Hangzhou 310018, P. R. China.*

This PDF file includes:

Experimental Section

Fig. S1 to S7

Tables S1-S2

Experimental Section

Synthesis of ATO/MWCNTs

Multi-walled carbon nanotubes (MWCNTs) used in this work were aminated.[1] Specifically, 100 mg of the aminated MWCNTs were dispersed in 30 mL of ethanol under ultrasonication. 20 mL of 0.315 M $SnCl_2$ (Macklin) in ethanol were then added under vigorous stirring. This was following by additional of 20 mL of 0.026 M $SbCl_3$ (Aladdin) in ethanol. The obtained homogeneous suspension was transferred into a 100 mL Teflon-lined autoclave and solvothermally heated at 150 ^oC for 3 h. The obtained ATO/MWCNTs precursor was washed by deionized (DI) water with sonication and dried at 70 ^oC overnight.

Synthesis of C@Sb-ATO/MWCNTs

30 mg of ATO/MWCNTs were dispersed into 30 mL of DI water containing 0.2 mL of pyrrole (Aladdin). After 30 min of sonication, 30 mL of 0.04 M $FeCl_3$ (Macklin) was added to the above mixture. After 4 h of stirring, the precipitates were washed with DI water and ethanol by centrifugation and dried at 70 ^oC overnight. The collected black solid was calcined at 450 °C for 2 h under the N_2 flow, which led to the formation of the C@Sb-ATO/MWCNTs.

For comparison, the C@SnO_2/MWCNTs was also prepared using the same synthetic procedure albeit in the absence of $SbCl_3$.

Materials characterization

The morphologies of the samples were observed by scanning electron microscopy (SEM, Merlin, Germany) and transmission electron microscopy (TEM, JEM-2100HR, Japan). Thermogravimetric analysis (TGA, Netzsch, Germany) was conducted on TGA/DSC 3+ from 30 ^oC to 700 ^oC under air atmosphere. The X-ray diffraction (XRD) patterns were obtained on the X-ray diffractomer (Bruker D8 Advance, Germany) using Cu Kα radiation. X-ray photoelectron (XPS) spectra were collected

on X-ray photoelectron spectrometer (ESCALAB 250, USA) with C 1s = 284.80 eV as the energy standard for binding energy calibration.

Electrochemical measurements

The anode slurry was prepared by mixing active material, carbon black and carboxyl methylated cellulose (CMC) in a mass ratio of 7: 2: 1 in water by ball-milling. The obtained slurry was cast on copper foil and dried at 80 °C for 12 h under vacuum. The mass loading of the active material was ~1.2 mg cm^{-2}. Electrochemical measurements were conducted by assembling the CR2032-type coin half-cells in an argon-filled glove box (O_2 < 0.1 ppm, H_2O < 0.1 ppm). The sodium metal was used as the counter electrode, the glass fiber (Whatman GF/D) as the separator, and $NaClO_4$ (1.0 M) dissolved in propylene carbonate (PC) containing 3 wt% fluoroethylene carbonate (FEC) as the electrolyte. The galvanostatic charge and discharge profiles under different current densities were measured on a LAND battery tester within a potential range of 0.01-3.0 V (vs. Na/Na^+) at room temperature. The Na^+ diffusion coefficient was measured by the galvanostatic intermittent titration method (GITT). Before testing, the working electrode was discharged/charged for 30 min and then aged for 2 h.

Cyclic voltammograms (CVs) were obtained on an Arbin battery tester within a potential range of 0.01-3.0 V. Electrochemical impedance spectra (EIS) were conducted on an electrochemical workstation (Solartron, 1260/1287) in the frequency range of 0.01 Hz to 100 kHz.

DFT calculations

The Vienna ab initio simulation package (VASP) using projector augmented wave method was employed to perform the DFT calculations.[2] The exchange–correlation interactions was described using the generalized gradient approximation in the form of Perdew-Burke-Ernzerhof.[3] A plane-wave cutoff energy was set to 450 eV. The DFT+U with U − J = 3.9 and 4.2 eV for Sn and Sb 4d orbitals

were used for all the calculations. The convergence criteria for energy and force were 1×10^{-5} and 0.05 eV $Å^{-1}$, respectively. The Γ-centered k-point mesh was used for the calculations. The climbing image NEB (CI-NEB) method[4] was used to calculated the energy barrier of Na diffusion. The Na binding energy (E_a) was calculated using:

$$E_a = E_{ATO/SnO_2\text{-}Na} - E_{ATO/SnO_2} - E_{Na} \quad \text{(S1)}$$

Where $E_{ATO/SnO_2\text{-}Na}$ is the total energy of Na adsorbed ATO or SnO_2, E_{ATO/SnO_2} is energy of ATO or SnO_2, and E_{Na} is the energy of sodium atom.

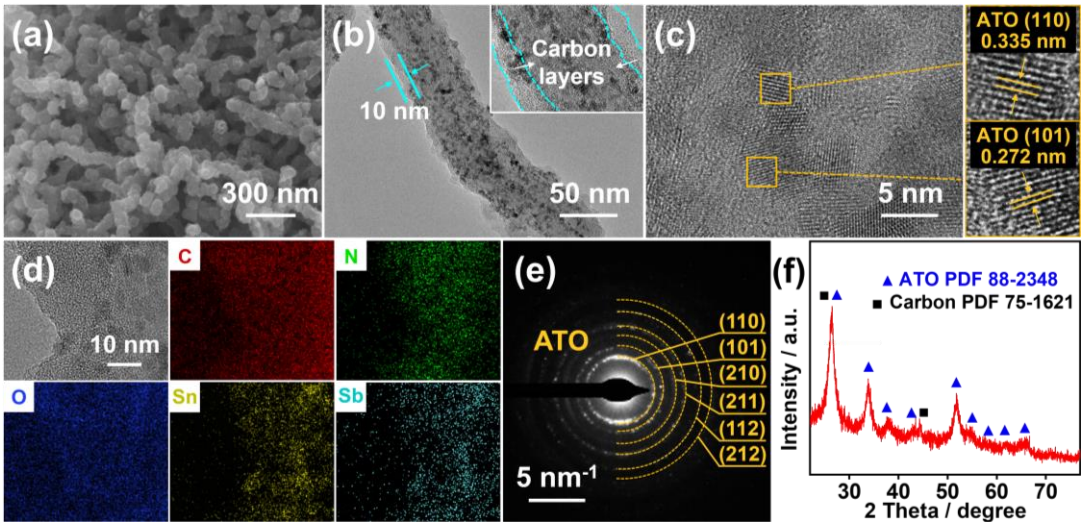

Fig. S1 (a) SEM and (b) TEM images of C@ATO/MWCNTs-etched. (c) HRTEM image of C@ATO/MWCNTs-etched. The right panel shows the magnified HRTEM images indicated. (d) Elemental mapping images, (e) SAED image and (f) XRD pattern of C@ATO/MWCNTs-etched.

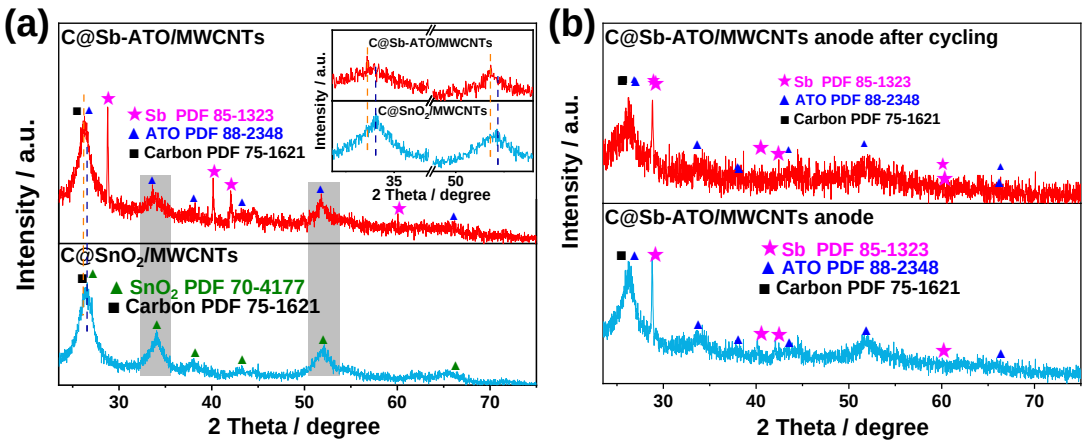

Fig. S2 (a) Comparison of the XRD patterns between C@Sb-ATO/MWCNTs and C@SnO_2/MWCNTs. The insets show the magnified XRD patterns marked gray. (b) Comparison of the XRD patterns of C@Sb-ATO/MWCNTs with binder and carbon black before and after 250 cycles.

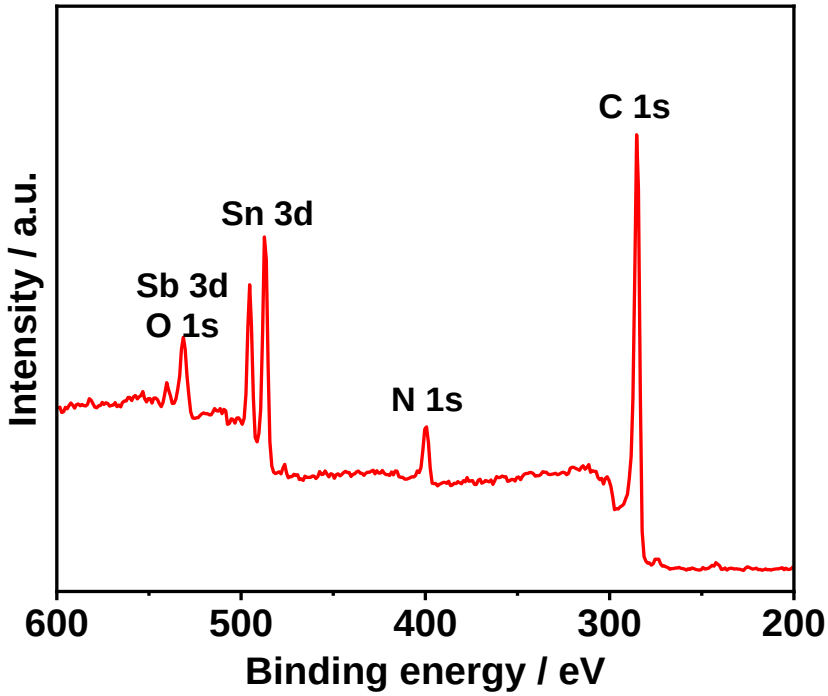

Fig. S3 XPS survey spectrum of C@Sb-ATO/MWCNTs.

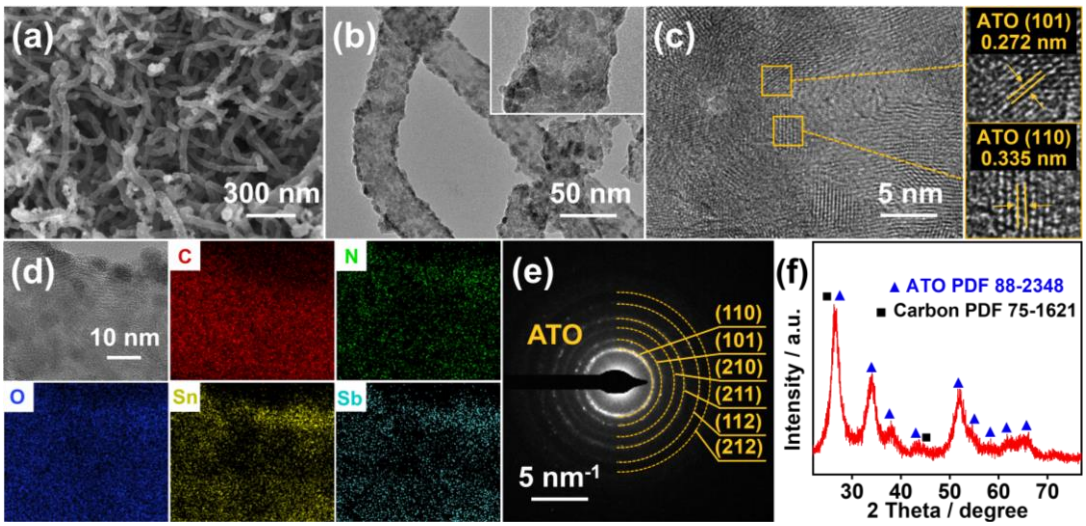

Fig. S4 (a) SEM and (b) TEM images of ATO/MWCNTs. (c) HRTEM image of ATO/MWCNTs. The right panel shows the magnified HRTEM images indicated. (d) Elemental mapping images, (e) SAED image and (f) XRD pattern of ATO/MWCNTs.

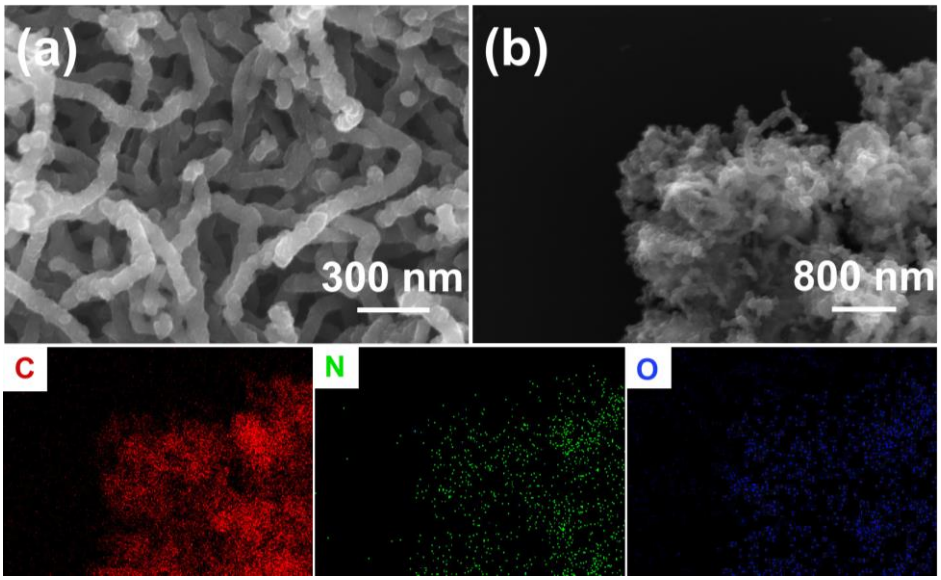

Fig. S5 (a) SEM image and (b) elemental mapping images of C@MWCNTs.

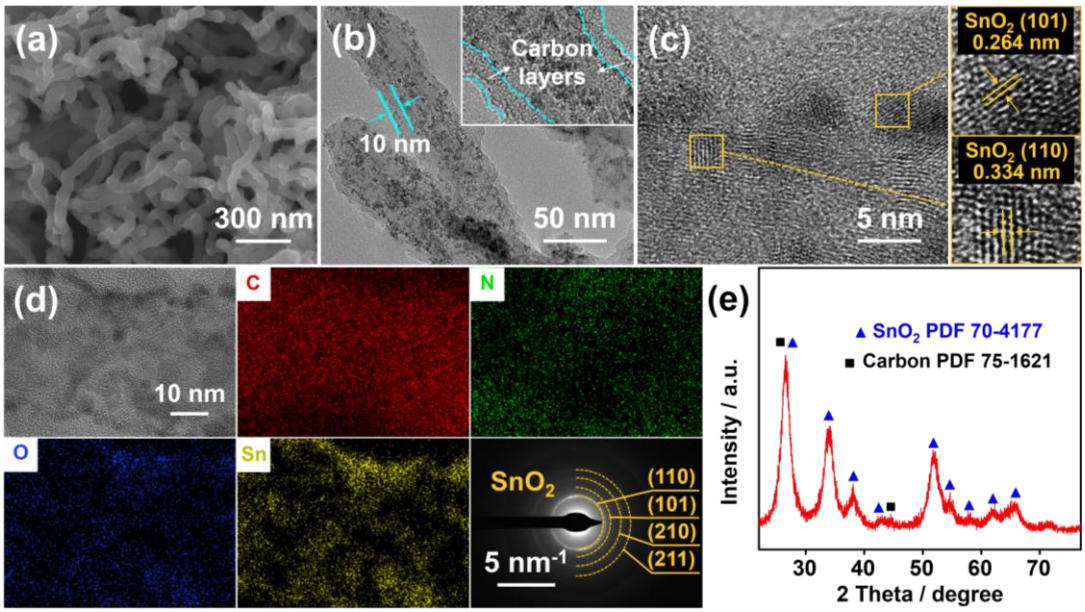

Fig. S6 (a) SEM and (b) TEM images of C@SnO_2/MWCNTs. (c) HRTEM image of C@SnO_2/MWCNTs. The right panel shows the magnified HRTEM images indicated. (d) Elemental mapping images and SAED image, (e) XRD pattern of C@SnO_2/MWCNTs.

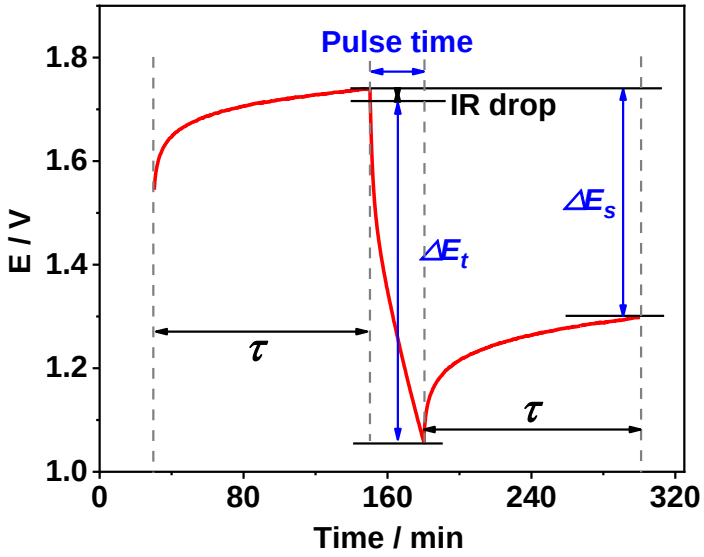

Fig. S7 *E* vs. *t* of C@Sb-ATO/MWCNTs for a single GITT pulse during discharge process.

The estimation of the Na^+ diffusion coefficient was done using the following equation:

$$D_{Na^+} = \frac{4}{\pi\tau}\left(\frac{mV_M}{M_w S}\right)^2\left(\frac{\Delta E_s}{\Delta E_t}\right)^2 \quad \text{(S2)}$$

Where m, V_M, and M_W stand for the mass, molar volume, molecular weight of the active material, respectively; τ is the relaxation time (**Fig. S7**); ΔE_s is the voltage variation at the steady states between two neighboring GITT curves (**Fig. S7**); ΔE_t is the total potential change with correction of the IR drop in a single current pulse (**Fig. S7**).

Table S1. Stable reversible capacity comparison of the C@Sb-ATO/MWCNTs with other anode materials for SIBs.

Electrode material	Mass loading mg cm^{-2}	Current density (mA g^{-1})	Cycles	Capacity (mAh g^{-1})	Ref.
C@Sb-ATO/MWCNTs	1.2	100	100	430.6	This work
		1000	4000	347.7	
		5000	10000	275.5	
SnO_2/NC	0.8~1.1	100	100	342.2	5
		1000	3000	212.6	
SnO_2		50	120	392.9	6
SnO_2@SnS_2@NG		3000	200	100	7
SnO_2/BTO@NCNF composite	0.88	5000	10000	183.4	8
SWCNTB@SnO_2@C		200	300	309	9
1T/2H MoS_2@SnO_2 heterostructure	1.2	2000	500	262	10
CC-SnO_2@PPy		100	300	403.7	11
SnO_2@hCNT		100	100	234	12
GN/SnO_2	1.0	100	100	290	13
SnO_2@TiO_2		100	100	222	14
SnSb@SnO_x/SbO_x@C	0.8-1.0	100	200	360	15
NiS@C/rGO		100	500	240.2	16
MXene@ReS_2@C	~1.0	200	200	202	17
$CoSe_2$/WSe_2@C/CNs	1.2	500	200	277	18
Cu-MoO_2@Mo_2C/NCNTs	1.1-1.3	2000	10000	195.5	19
DMcT-MoO_3		5000	1200	105	20
Fe_7Se_8@C@$MoSe_2$		1000	600	345	21
Co_9S_8/HNCS		1000	300	224	22
NiS@NCNT microspheres		1000	500	289.8	23
FeP@NPC		1000	300	253	24
Co_2P/Sn@NC	~1.0	5000	10000	168	25
N, B co-doping carbon nanosheets		200	200	309	26
		1000	2000	225	
Ti_3C_2/NiCoP	1.0	1000	2000	261.7	27
Bi@Graphite	~0.5	3200	10000	142	28

Table S2. Rate performance comparison of the C@Sb-ATO/MWCNTs with other materials for SIBs.

Electrode material	Mass loading mg cm^{-2}	0.1 A g^{-1}	0.2 A g^{-1}	0.5 A g^{-1}	1.0 A g^{-1}	2.0 A g^{-1}	5.0 A g^{-1}	10.0 A g^{-1}	20.0 A g^{-1}	30.0 A g^{-1}	Ref.
C@Sb-ATO/MWCNTs	1.2	432.0	402.8	376.2	344.6	311.5	263.5	229.1	217.5	198.5	This work
SnO_2/NC	0.8~1.1	344.3	312.2	269.2	236.5	194.9					5
SnO_2		376.2	328.9	274.3	222.2	168.9					6
SnO_2@hCNT		255	226	207	188	170					12
GN/SnO_2		315	280		166	128					13
SnO_2@TiO_2		309.8	244.8								14
SnSb@SnO_x/SbO_x@C	0.8-1.0			332.7	325.4	293.3	244.3	180.5			15
MXene@ReS_2@C	~1.0	323	283	253	233	204	138				17
Cu-MoO_2@Mo_2C/NCNTs	1.1-1.3	376.9	330.5	289.4	240.1	202.5	180.3				19
DMcT-MoO_3		296	256	229	205	179	127				20
Co_9S_8/HNCS		386	340		311	288	252				22
Co_2P/Sn@NC	~1.0	394	336	291	264	233		147			25
N, B co-doping carbon nanosheets		310	290	260	217	200	196	192			26
SnO_2 NRs/GA	1-2	208		141	111						29
Multishelled Fe_2O_3@SnO_2@C nanotubes	~1.5	374.6	305.7		135.4						30
CNTs@SnO_2@G		247	221		97						31
SnO_2@FeOOH@C	0.5	398.2	390.9		315.5	275.6	211.4				32
Sb_2O_3@Sb@NC	0.6-0.8	343.8	307.1					175.1			33
YS-Cu-FeP@C	1.0	406	387	342	302	260	188	145			34
CoP/FeP@PCNF	1.0	424			356		261	213			26

References

1. B. Deng, D. Wang, Z. Jiang, J. Zhang, S. Shi, Z.-J. Jiang and M. Liu, *Carbon*, 2018, **138**, 169-178.
2. G. Kresse and J. Furthmüller, *Phys. Rev. B*, 1996, **54**, 11169-11186.
3. J. P. Perdew, K. Burke and M. Ernzerhof, *Phys. Rev. Lett.*, 1996, **77**, 3865-3868.
4. G. Henkelman, B. P. Uberuaga and H. Jonsson, *J. Chem. Phys.*, 2000, **113**, 9901-9904.
5. Y. Cheng, S. Wang, L. Zhou, L. Chang, W. Liu, D. Yin, Z. Yi and L. Wang, *Small*, 2020, **16**, 2000681.

6. H.-g. Wang, Q. Wu, Y. Wang, X. Wang, L. Wu, S. Song and H. Zhang, *Adv. Energy Mater.*, 2019, **9**, 1802993.
7. S. Huang, M. Wang, P. Jia, B. Wang, J. Zhang and Y. Zhao, *Energy Storage Mater.*, 2019, **20**, 225-233.
8. R. Li, G. Zhang, Y. Wang, Z. Lin, C. He, Y. Li, X. Ren, P. Zhang and H. Mi, *Nano Energy*, 2021, **90**, 106591.
9. Y. Wang, J. Ren, X. Gao, W. Zhang, H. Duan, M. Wang, J. Shui and M. Xu, *Small*, 2018, **14**, 1802913.
10. D. Gui, Z. Wei, J. Chen, L. Yan, J. Li, P. Zhang and C. Zhao, *J. Mater. Chem. A*, 2021, **9**, 463-471.
11. M. Wang, X. Wang, Z. Yao, W. Tang, X. Xia, C. Gu and J. Tu, *ACS Appl. Mater. Interfaces*, 2019, **11**, 24198-24204.
12. M. Li, F. Luo, Q. Zhang, Z. Yang and Z. Xu, *J. Catal.*, 2020, **381**, 395-401.
13. Y. Li, Y. Zhao, C. Ma, J. Shi and Y. Zhao, *J. Alloys Compd.*, 2020, **821**, 153506.
14. J. Liang, L. Zhang, D. XiLi and J. Kang, *Electrochim. Acta*, 2020, **341**, 136030.
15. Z. Wang, K. Dong, D. Wang, F. Chen, S. Luo, Y. Liu, C. He, C. Shi and N. Zhao, *Chem. Eng. J.*, 2019, **371**, 356-365.
16. Z. Song, G. Wang, Y. Chen, Q. Chang, Y. Lu and Z. Wen, *Chem. Eng. J.*, 2022, **435**, 134633.
17. X. Liu, M. Wang, B. Qin, Y. Zhang, Z. Liu and H. Fan, *Chem. Eng. J.*, 2022, **431**, 133796.
18. W. Chen, W. Wei, K. Wang, N. Zhang, G. Chen, Y. Hu and K. Ostrikov, *Nanoscale*, 2021, **13**, 6201-6211.
19. S. Yang, C. Liu, H. Li, S. Wang, J. Choi and L. Li, *Energy Storage Mater.*, 2021, **39**, 278-286.
20. B. Wang, E. H. Ang, Y. Yang, Y. Zhang, H. Geng, M. Ye and C. C. Li, *Adv. Funct. Mater.*, 2020, **30**, 2001708.
21. H. Fan, W. Chen, G. Chen, J. Huang, C. Song, Y. Du, C. Li and K. Ostrikov, *Appl. Catal. B: Environ.*, 2020, **268**, 118440.

22. H. Shangguan, W. Huang, C. Engelbrekt, X. Zheng, F. Shen, X. Xiao, L. Ci, P. Si and J. Zhang, *Energy Storage Mater.*, 2019, **18**, 114-124.
23. S. Fan, S. Huang, Y. Chen, Y. Shang, Y. Wang, D. Kong, M. E. Pam, L. Shi, Y. W. Lim, Y. Shi and H. Y. Yang, *Energy Storage Mater.*, 2019, **23**, 17-24.
24. S. Shi, Z. Li, L. Shen, X. Yin, Y. Liu, G. Chang, J. Wang, S. Xu, J. Zhang and Y. Zhao, *Energy Storage Mater.*, 2020, **29**, 78-83.
25. X. Ren, Z. Ren, Q. Li, W. Wen, X. Li, Y. Chen, L. Xie, L. Zhang, D. Zhu, B. Gao, P. K. Chu and K. Huo, *Adv. Energy Mater.*, 2019, **9**, 1900091.
26. Q. Jin, W. Li, K. Wang, H. Li, P. Feng, Z. Zhang, W. Wang and K. Jiang, *Adv. Funct. Mater.*, 2020, **30**, 1909907.
27. D. Zhao, R. Zhao, S. Dong, X. Miao, Z. Zhang, C. Wang and L. Yin, *Energy Environ. Sci.*, 2019, **12**, 2422-2432.
28. J. Chen, X. Fan, X. Ji, T. Gao, S. Hou, X. Zhou, L. Wang, F. Wang, C. Yang, L. Chen and C. Wang, *Energy Environ. Sci.*, 2018, **11**, 1218-1225.
29. Y. Wang, Y. Jin, C. Zhao, E. Pan and M. Jia, *J. Colloid Interface Sci.*, 2018, **532**, 352-362.
30. F. Li, G. Luo, W. Chen, Y. Chen, Y. Fang, M. Zheng and X. Yu, *ACS Appl. Mater. Interfaces*, 2019, **11**, 36949-36959.
31. D. Zhou, X. Li, L.-Z. Fan and Y. Deng, *Electrochim. Acta*, 2017, **230**, 212-221.
32. Z. Zhao, H. Su, S. Li, C. Li, Z. Liu and D. Li, *J. Alloys Compd.*, 2020, **838**, 155394.
33. A. Xu, C. Huang, G. Li, K. Zou, H. Sun, L. Fu, J. Ju, Y. Song, S. Wu, Z. Xu and Y. Yan, *J. Mater. Chem. A*, 2021, **9**, 12169-12178.
34. J. Li, Q. Liu, Y. Zhang, J. Jiang, H. B. Wu and X.-Y. Yu, *Chem. Eng. J.*, 2020, 127776.